Food Chemistry: X 22 (2024) 101350

Contents lists available at ScienceDirect

Food Chemistry: X

journal homepage: www.sciencedirect.com/journal/food-chemistry-x

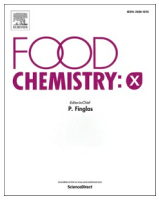

Dry fractionation efficiency of milk fats from different sources and the characteristics of their fractions in chemical composition, thermal property, and crystal morphology

Yue Li [a], Yan Li [b,*], Guosen Yan [a], Shiran Wang [a], Yunna Wang [c], Yang Li [a], Zhenbo Shao [a], Hui Wang [b], Liebing Zhang [a]

[a] College of Food Science and Nutritional Engineering, China Agricultural University, Beijing 100083, China
[b] Beijing Engineering and Technology Research Centre of Food Additives, School of Food and Health, Beijing Technology and Business University, Beijing 100048, China
[c] Institute of Food Science and Technology, Chinese Academy of Agricultural Sciences, Beijing 100193, China

ARTICLE INFO

Keywords:
Milk fat
Dry fractionation efficiency
Chemical composition
Thermal properties
Crystallization

ABSTRACT

The physicochemical properties of anhydrous milk fats (AMF) often change according to different regions and seasons, inevitably affecting dry fractionation. This study analyzed the differences in the fraction yields and physicochemical characteristics of four AMFs from different sources. The results showed that single-stage dry fractionation conducted at 25 °C easily separated AMFs into liquid fractions (L25) and solid fractions (S25) via pressure filtration, both producing satisfactory yields. Moreover, all L25s exhibited few crystals with good fluidity at 25 °C, while S25s presented as semi-solids supported by β crystal networks with a certain hardness and plasticity. However, four AMFs displayed fractionation efficiency variation, while the thermal differences among them showed no obvious correlation with those among their fractions. Generally, more trisaturated triglycerides with 48 to 54 carbon atoms in the AMF increased the S25 yield and decreased the slip melting points (SMP) of both fractions.

1. Introduction

Milk fat (MF), a natural product separated from milk, is essential for the flavor, nutritional, and functional characteristics of dairy products. MF mainly comprises triglycerides (TAG, about 98% of the total lipids), phospholipids, sterols, free fatty acids, and fat-soluble vitamins. >400 fatty acids (FA) with different chain lengths and saturation degrees are combined into complex TAG mixtures according to different sn-position distribution, resulting in MF with a wide melting range between −40 °C and 40 °C (Fatouh, Singh, Koehler, Mahran, & Metwally, 2005; Si et al., 2023). Although its unique flavor, texture, and nutritional value make MF an ideal ingredient for many foods (Wang et al., 2023; Yan et al., 2023), it presents some challenges regarding quality stability. The chemical composition of MF often fluctuates due to influencing factors, such as bovine species, lactation stages, nutritional feed values, regions, and seasons, changing its physical properties like crystallization and melting behavior (Chilliard, Ferlay, & Doreau, 2001; Larsen, Andersen, Kaufmann, & Wiking, 2014; Maurice-Van, Hiemstra, & Calus, 2011; Pacheco-Pappenheim et al., 2022). Consequently, modifying MF offers a useful technique to preserve MF quality stability and enhance its functional qualities.

Dry fractionation is a green, clean, additive-free modification technology that can separate MF into fractions with different melting point (MP) ranges and functional properties by controlling the fractionation temperature. It retains the flavor and nutrients of natural MF and expands its application scope, increasing the targeted utilization of MF fractions (Yener & van Valenberg, 2019). The physicochemical characteristics of various MF fractions produced via dry fractionation have been continually studied over the past few decades, yielding various study methodologies. Fatouh et al. (2003) fractionated buffalo butter oil at temperatures between 15 °C ~ 40 °C via stepwise crystallization and determined the FA composition and thermal profile of each fraction using gas chromatography (GC) and differential scanning calorimetry (DSC), respectively. The results showed long-chain saturated FAs (LC-SFA) enrichment in high melting fractions (HMF), while short-chain FAs (SC-FA) and unsaturated FAs (USFA) were mainly presented in low melting fractions (LMF), and the FA composition of middle melting fractions (MMF) existed between LMF and HMF. HMFs displayed

* Corresponding author.
E-mail address: liyan@btbu.edu.cn (Y. Li).

https://doi.org/10.1016/j.fochx.2024.101350
Received 4 December 2023; Received in revised form 25 February 2024; Accepted 1 April 2024
Available online 2 April 2024

significantly higher melting characteristics than LMF. Lopez, Bourgaux, Lesieur, Riaublanc, and Ollivon (2006) used high-performance liquid chromatography (HPLC) to examine the differences between MF and its fractions in TAG compositions after fractionation at 21 °C while investigating the crystallization properties via DSC and synchrotron X-ray diffraction. The results showed that TAGs rich in SC-FAs and USFAs were higher in the olein fraction, while TAGs rich in LC-FAs and SFA were higher in the stearin fraction. MF and the olein fraction mainly crystallized as α crystals at low temperatures, while the stearin fraction formed mixed α and β' crystals. Lopez and Ollivon (2009) examined polymorphic fat crystal evolution, indicating a polymorphic α → β' transition in each fraction on heating. Wang et al. (2019) conducted dry fractionation on MF between 20 °C and 40 °C, first performing heating, followed by cooling. The results indicated that the significant alteration in the chemical compositions of the fractions substantially changed their physical properties, of which promising plasticity was shown in the high solid fat content of the HMFs.

All these studies used MF from single sources, analyzing the chemical composition, thermal, and crystallization characteristics of the fractions longitudinally. However, minimal studies are available regarding the chemical composition variation of MFs according to regional and seasonal factors, which inevitably affect their dry fractionation efficiency. Moreover, the dry fractionation processes used in different studies vary significantly. The fractionation process is divided into single-stage and multistage fractionation. Multistage fractionation involves using heating, cooling, or a combination of the two for finer fractions. Furthermore, the cooling rate and constant temperature time also lead to different fat crystal types, while the solid and liquid fraction separation methods, such as vacuum, pressure, and centrifugal filtration, affect the yield and composition (Fatouh et al., 2003; Małkowska, Staniewski, & Ziajka, 2021; Si et al., 2023; Wang et al., 2019). The inconsistency of dry fractionation methods in different studies made obtaining a set of standardized processes in the industry difficult. Furthermore, it is difficult to identify similar fractions for physicochemical property variation comparison to learn more about the effect of dry fractionation on MFs from different sources.

Therefore, this study explores the variation in the fractionation temperatures and fraction yield of four AMFs from different sources and analyzes the chemical compositions, thermal properties, and crystal morphology of the subsequent fractions. This can provide valuable data for the application of MF dry fractionation.

2. Materials and methods

2.1. Preparation of the AMF

This experiment used four butter brands from different countries. Butter A was purchased from Inner Mongolia Mengniu Cheese Co. Ltd. (China). Butter B was obtained from Fonterra Cooperative Group (New Zealand). Butter C was acquired from Shanghai Goff Foods Co. Ltd. (China, origin Argentina). Butter D was purchased from J.F. Vegt Holding B.V. (Netherlands).

The AMF was prepared using a method described by Precht, Molkentin, and de Froidmont-Gortz (1998) with minor modifications. The butter was completely melted at 60 °C in an oven, and the top fat layer was filtered out using mesh. The fat was washed with water and left to stand at 60 °C for 30 min, after which the bottom water phase was separated and washed again. The AMF (water content <0.02%) was obtained via evaporation in a vacuum gyroscope at 60 °C until no steam emerged, cooled to room temperature, and refrigerated at 4 °C for use.

2.2. Dry fractionation process

2.2.1. Multistage dry fractionation via heating

The dry fractionation temperatures were between 20 °C and 30 °C. Approximately 200 g of the AMF was completely melted in a water bath at 50 °C and crystallized at 20 °C for a holding time of 12 h. The subsequent solid fraction (S20) was separated from the liquid fraction (L20) via pressure filtration using an oil compressor and nylon mesh. After implementing the same holding time at 30 °C, the S20 was further fractionated to obtain the S30 and L30 solid and liquid fractions via vacuum filtration.

2.2.2. Multistage dry fractionation via cooling

After implementing the same melting procedure and holding time, the AMF was fractionated at 30 °C to acquire the S30 and L30 solid and liquid fractions via vacuum filtration. Then, L30 was crystallized at 20 °C for 12 h to obtain the S20 and L20 solid and liquid fractions via pressure filtration.

2.2.3. Single-stage dry fractionation

The same melting procedure and holding time were adopted. The AMF was fractionated at 25 °C to generate the S25 and L25 solid and liquid fractions by via pressure filtration.

Solid and liquid fractions were weighed, and each yield was calculated.

$$\text{Solid fraction}\ (\%) = \frac{\text{Solid weight}}{\text{AMF weight}} \times 100\% \quad (1)$$

$$\text{Liquid fraction}\ (\%) = 1 - \text{Solid fraction}\% \quad (2)$$

2.3. Slip melting point (SMP)

The SMPs of the AMFs and fractions were determined according to the description of Si et al. (2023).

2.4. Thermal behavior

The non-isothermal melting and crystallization behavior of the AMF and fractions were assessed via DSC 214 Polyma (Netzsch, Selb, Germany), and the Proteus Analysis Software Version 7.0.1 was used for the thermal sample analysis. About 10 mg of the sample was added to a DSC aluminum pan and sealed, with an empty pan as the control. The samples were rapidly heated from room temperature to 80 °C (100 °C /min) and maintained for 3 min to eliminate historical crystallization. Then, the samples were cooled at 5 °C/min to −20 °C and maintained for 2 min, after which the temperature was increased to 50 °C at 5 °C/min. The curve of the heat flow (w/g) with the temperature during crystallization and melting was recorded (Wang et al., 2019).

2.5. FA composition

The fatty acid methyl esters (FAME) were prepared referring to the method of Wang et al. (2019), with minor alternations. Specifically, 100 mg–200 mg of AMF was weighed and added to a 1.0 mL pyrogallic acid methanol solution (10%), followed by a 10 mL potassium hydroxide methanol solution (0.5 mol/L) and a 2 mL methyl enanthate internal standard solution (5 mg/mL). The mixture was heated in a water bath at 80 ± 1 °C with condensation reflux for 5 min ~ 10 min. Then, a 5 mL 14% boron trifluoride methanol solution was added, and reflux was continued for 15 min, after which the mixture was cooled to room temperature. The liquid was transferred from the flask into a 50 mL centrifuge tube. The flask was cleaned three times using a 3 mL saturated sodium chloride solution, which was subsequently added to the 50 mL centrifuge tube. Next, 10 mL n-hexane was added to the tube and shaken, followed by centrifugation at 5000 r/min for 5 min, after which the supernatant was collected for determination.

A 1 μL sample was injected into a gas chromatography–mass spectrometry (GC–MS, 7890B-5977B, Agilent) DB-WAX capillary column (30 m × 250 μm × 0.25 μm) equipped with a flame-ionization detector (FID) for analysis. The parameters included an inlet temperature of

250 °C, a split ratio of 1:10, and a carrier gas flow rate of 1 mL/min. The oven temperature started at 35 °C, which was maintained for 5 min. The temperature was then increased at 10 °C/min to 175 °C and maintained for 1 min, followed by an increase to 205 °C at 1.5 °C/min and maintained for 1 min. Finally, the temperature was raised to 230 °C at 5 °C/min. The mass spectrometer was operated in electron ionization mode at 70 eV. Scan mode was used for analysis (mass range between *m/z* 30 to 500). Data were collected using the Mass Hunter 0.7.0.0 software, and FAs were identified as their methyl esters by using a NIST library (Shimadzu, Kyoto, Japan). The quantification was performed with the internal standard together with experimentally determined response factors. The identification details were shown in **Table S2**. The FA composition of the AMF was calculated as the L25 and S25 yield ratio.

2.6. TAG profile

A 10-mg sample was dissolved in a methylene chloride and isopropyl alcohol mixture (1:1, v:v) to produce a 10 mg/mL sample reserve solution. Next, 12:0 Lyso PC (LPC 12:0) (Avanti) was dissolved in an isopropyl alcohol-acetonitrile solution (9:1, v:v) to obtain a 1 μM LPC 12:0 internal standard solution. The sample reserve solution was diluted 100 times using an internal standard mixture for liquid chromatography-mass spectrometry (LC-MS) analysis.

A 5-μL sample was loaded into an LC system (I-class Acquity ultra-performance liquid chromatography, Waters) equipped with a BEH C18 column (1.7 μm, 2.1 mm × 100 mm, WATERS). Mobile phase A consisted of isopropanol-acetonitrile (9:1, v:v), while mobile phase B comprised acetonitrile and water (1:1, v:v), both containing 0.1% formic acid and 10 mM ammonium formate. The column temperature was set to 60 °C, and the flow rate was 300 μL/min. The gradient elution process followed as 75% A and 25% B for 0 min, 85% A and 15% B for 16 min, 75% A and 25% B for 16.1 min, and 75% A and 25% B for 18 min.

An API 4500 QTRAP mass spectrometer (MDS SCIEX) equipped with an electrospray ionization (ESI) source was used for MS analysis. All experiments were conducted in positive ionization mode. The specific parameters included an IonSpray Voltage (IS) of 5500 V, a temperature (TEM) of 550 °C, an ion source gas1 (GAS1) of 45 psi, an ion source gas2 (GAS2) of 50 psi, and a curtain gas (CUR) of 30 psi. The scan mode was used to obtain all all precursor ion information of TAGs, and declustering potential (DP) was set at 120 V. For the product ion scan (PIS) mode, the multiple response monitoring (MRM) (Q1 = Q3) - information dependent acquisition (IDA) - enhancement product ion (EPI) mode were established for the qualification of TAGs with specific fatty acyl chains, and the collision energy (CE) was set at 7 V. For the quantification of individual TAG with specific fatty acyl chains, MRM (Q1 ≠ Q3) mode was created and the collision energy was set as 45 V. The specific method was referred to the description of Guan et al. (2017) and the identification details were shown in **Table S3**. The TAG profile of the AMF was calculated as the L25 and S25 yield ratio.

2.7. Crystal morphology

The isothermal crystal morphology of the AMFs and fractions was observed using a polarizing microscope (BX53, Olympus, Japan). The samples were heated to 60 °C to melt completely, diluted with preheated vegetable oil to different concentrations (15 °C, AMF: 2×, S25: 5×; 25 °C, S25: 3×; × represents dilution times), and vortex mixing to obtain diluted samples. The samples and diluted samples (about 10 μL) were dropped onto a circular glass slide, concentrically covered with a smaller coverslip, and then maintained at 15 °C and 25 °C, respectively, for 24 h. The temperature controller (RTL150/B, HZ instruments, China) was adjusted, and the sample was observed at 10 × 10 magnification. At least five images of each sample were taken (Yao et al., 2020).

2.8. Statistical analysis

All measurements were performed in triplicate. The data were reported as mean ± standard deviation and assessed via one-way analysis of variance (ANOVA) using IBM SPSS 26 (Chicago, USA), with $p < 0.05$ considered statistically significant. The figures were plotted using Origin 2022b (OriginLab, USA).

3. Results and discussion

3.1. Efficiency of dry fractionation

The DSC melting curves of the four AMFs (Fig. 1a) exhibited three typical endothermic peaks in distinct temperature regions, including low endothermic peaks (LEP) between 0 °C and 14 °C, medium endothermic peaks (MEP) between 14 °C and 20 °C, and high endothermic peaks (HEP) between 20 °C and 40 °C (Sebben, Gao, Gillies, Beattie, & Krasowska, 2019). During cooling (Fig. 1A), all four AMFs crystallized at about 16 °C, displaying two exothermic crystallization peaks (Si et al., 2023). Since the division of the different fractions in crystallization curves was unclear, the melting curves were used to determine the dry fractionation temperature nodes. The LMF separation node was set to 20 °C due to the narrow LEP and MEP melting ranges, which all ended before 20 °C. Since the HEPs displayed a broader melting range and area, 30 °C was used as the separation node of MMF and HMF. Multistage dry fractionation using a heating program was conducted first. The S30 yields were the highest, all exceeding 50%, followed by the L20s at about 35%, while those of the L30s were the lowest at below 10% (Fig. 1B). Moreover, the S20s appeared mushy after exposure to 30 °C for 12 h, which made L30 separation difficult, even via vacuum filtration. The S30s subjected to multistage dry fractionation using a cooling program displayed similar results, with A-S30 and D-S30 yields below 10% (data not provided). Single-stage dry fractionation at 25 °C was used to separate the S25s and L25s via pressure extrusion. The four AMFs presented distinctly different fraction yields (Fig. 1b). The yields of the four L25s all exceeded 50%, following an order of B-L25 ≈ C-L25<D-L25<A-L25 ($P < 0.05$), while the yields of the four S25s were below those of the L25s. Even B-S25 and C-S25, which exhibited the lowest yields, exceeded 30%. Therefore, since single-stage dry fractionation at 25 °C was more suitable for large-scale production, it was adopted in this study for further research.

3.2. Thermal properties

The SMP of A-AMF was the highest among the AMFs, while those of A-L25 and A-S25 were the lowest among the L25s and S25s, respectively (Fig. 2A). Furthermore, the A-AMF exhibited the highest T_{Con} and T_{Mend} in the AMF DSC curves, while A-L25 and A-S25 showed the lowest HEP values and T_{Mend} in the respective fractions (**Table S1**). The SMP of the B-AMF was only second to the A-AMF, while those of B-L25 and B-S25 were highest among their respective fractions. According to the DSC curves, B-L25 also showed the highest T_{Mend} among the four L25s, which did not melt completely until 26.86 °C, while B-S25 showed the highest HEP values and the steepest shape of the four S25s (Figs. 2b and c). The SMPs of the C-AMF and D-AMF were the lowest of the four AMFs, while their fractions were in the middle. This showed that there was no obvious correlation between the thermal property trends of the different AMFs and those of L25s and S25s obtained via dry fractionation.

The AMF fraction yields indicated that a higher S25 yield decreased the SMPs of both fractions, which could be explained by the findings of Yao et al. (2020), who showed that although extended crystallization time increased the crystal content separated from cocoa butter, the MPs decreased, due to the participation of more low-melting TAGs. Therefore, a higher S25 yield meant the presence of more co-crystallized low-melting TAGs, which were less in L25s, decreasing the SMPs of both fractions.

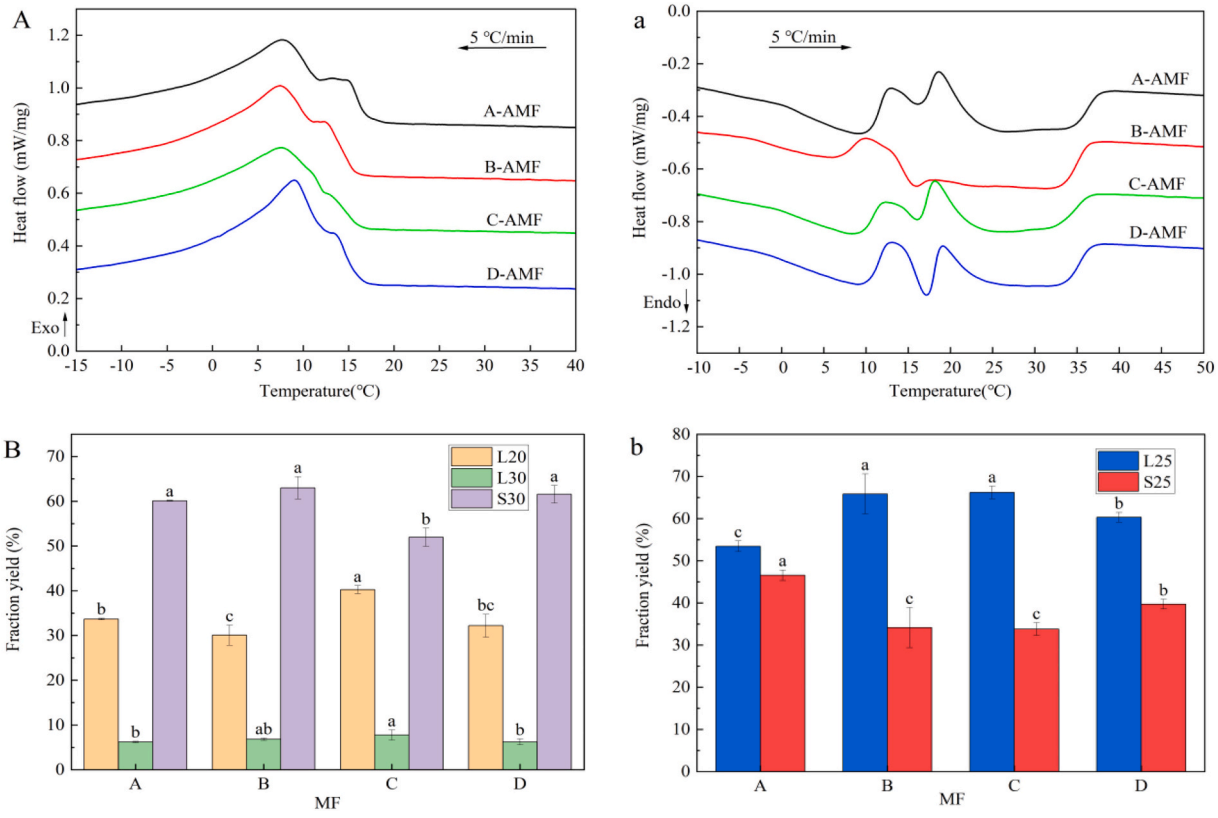

Fig. 1. The crystallization (A) and melting (a) curves of the AMFs from different sources and the yields of each fraction (B and b).

Although some thermal property differences were evident between the four AMFs and their fractions, the SMPs of the L25s were all lower than 25 °C, while their HEPs showed a narrower temperature range than the AMFs (Fig. 2b). Therefore, as the temperature increased to around 25 °C, the L25 quickly changed into a liquid state. The T_{Con} of each L25 was delayed to about 10 °C compared to the AMFs, while only a single exothermic crystallization peak was recorded at 8 °C ~ 10 °C (Fig. 2B). The S25s all showed higher SMPs than the AMFs, while their HEPs were significantly broader and skewed to the right, and their T_{Mend} values all exceeded 40 °C (Fig. 2c), indicating that the change process of the S25s from a solid to a liquid phase was relatively slow. The T_{Con} values of the S25s increased to about 23 °C, with three exothermal peaks appearing at 20 °C ~ 22 °C, 13 °C ~ 15 °C, and 10 °C ~ 12 °C, respectively (Fig. 2C). The results showed that the same fractions obtained from the four different AMFs via single-stage dry fractionation showed similar thermal states at 25 °C, of which the L25s maintained a liquid with good fluidity, while the S25s were semi-solid with a certain hardness and plasticity.

3.3. Chemical composition

3.3.1. FA composition

FAs are important components of TAGs, significantly affecting the thermal and crystal properties of MF and playing a vital role in the fractionation process (Himawan, Starov, & Stapley, 2006; Si et al., 2023). Although the FA compositions were similar in the four AMFs and fractions, some differences were exsited in the content (Table 1).

The FAs were classified into four major groups based on chain length and saturation, including short-chain saturated FAs (SC-SFA, C4:0 ~ C6:0), medium-chain saturated FAs (MC-SFA, C8:0 ~ C12:0), LC-SFAs (C13:0), and USFAs (Ren, Li, Dudu, & Ma, 2019). The four AMFs all primarily contained LC-SFAs, accounting for about 50%, of which palmitic acid (C16:0) was the most abundant at >20%, followed by stearic acid (C18:0) and myristic acid (C14:0). The USFA content was second only to LC-SFA at about 40%, which was especially rich in oleic acid (C18:1). SC-SFA and MC-SFA were less abundant at 4% and 10%, respectively. A longer FA carbon chain increased the MP. When the carbon chain lengths were identical, the FA with high saturation displayed higher MP (Wang et al., 2019). The A-AMF displayed the highest stearic and oleic acid levels and SMP values, while the other three AMFs exhibited higher SC- and MC-SFA levels and lower SMP values ($P<0.05$). The D-AMF contained the most LC-SFA, mainly composed of C14:0-C17:0, but showed the lowest SMP, inferring that stearic acid and oleic acid had a more significant impact on the SMP than other LC-SFAs.

Higher SC-SFA, MC-SFA, and USFA levels and lower LC-SFA content were evident in the four L25s, while the S25s displayed an opposite trend. This was because SC-SFA, MC-SFA, and USFA were prone to the presence in low-melting TAGs that mostly remained in L25s during fractionation, while LC-SFA tended to consititude high-melting TAGs that was enriched in the S25s. Furthermore, each S25 retained FA composition characteristics similar to its AMF. For instance, the A-S25 displayed the highest stearic and oleic acid content, while the D-S25 showed the most abundant LC-SFA level. The four L25s displayed fewer FA content differences than the AMFs, and no significant differences were evident in the SC-SFA, MC-SFA, and USFA levels ($P>0.05$). This was possibly due to the lowest A-L25 yield, increasing its SC-SFA, MC-SFA, and USFA proportions.

3.3.2. TAG profile

MF is considered the most complex natural fat, largely due to TAG diversity, with over 200 TAGs reportedly detected in MF (Gresti, Bugaut, Maniongui, & Bezard, 1993; Lopez et al., 2006). In addition, compared to the simple FA composition analysis, the TAG profile could more directly and accurately reflect the physical properties of MF. This study selected 71 high-content TAGs for statistical analysis, which were plotted into a heat diagram (Table 2 **and** Fig. 3).

According to their saturation and molecular weight, these TAGs were classified into trisaturated TAGs with 41 to 54 carbon atoms (HMW-S3-TAG), trisaturated TAGs with 26 to 40 carbon atoms (LMMW-S3-TAG),

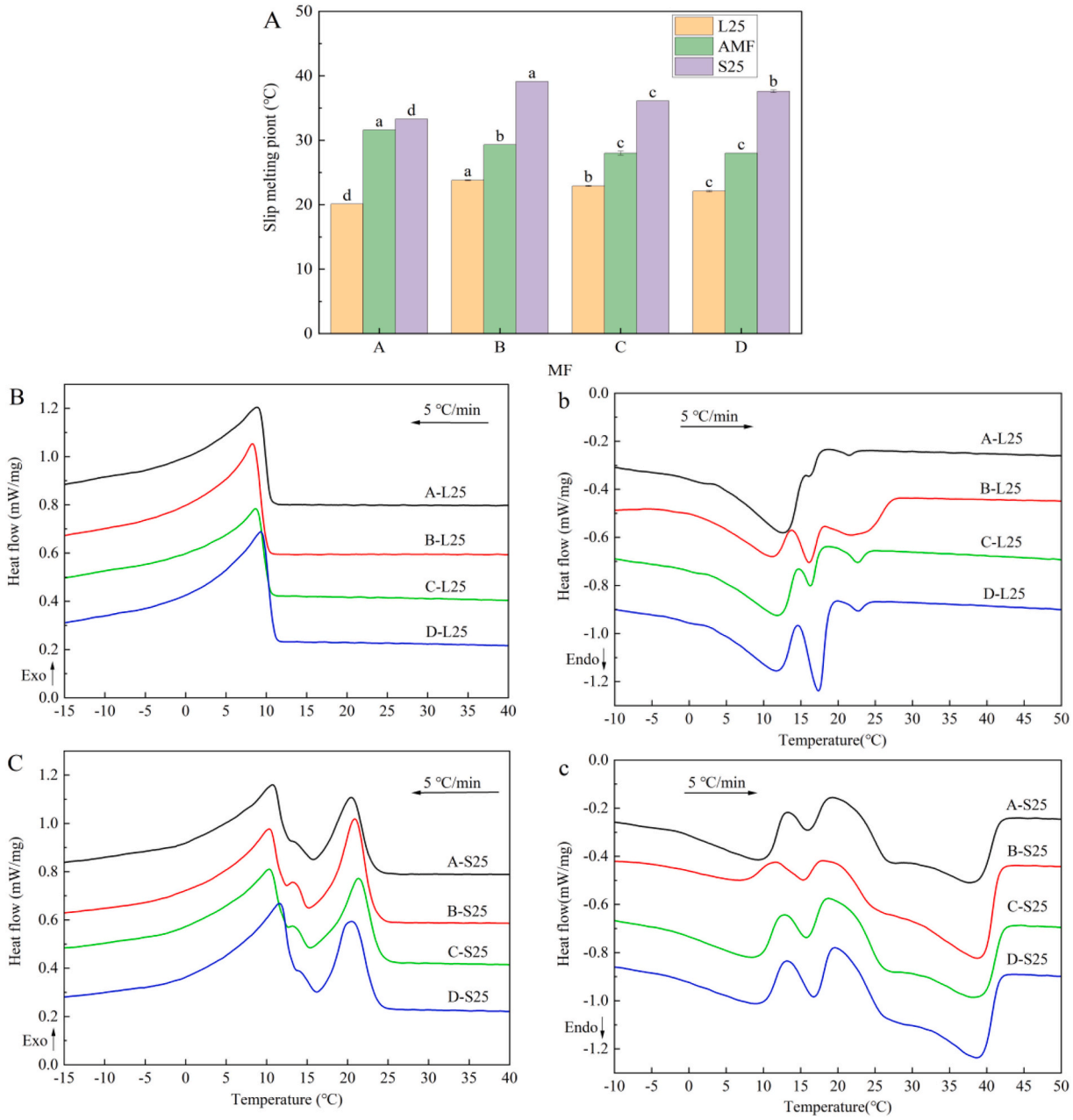

Fig. 2. The SMPs (A) and DSC crystallization (B, C) melting (b, c) curves of the MFs from different sources and their fractions.

monounsaturated TAGs with 41 to 54 carbon atoms (HMW-S2U1-TAG), monounsaturated TAGs with 28 to 40 carbon atoms (LMMW-S2U1-TAG), diunsaturated TAGs (S1U2-TAG), and triunsaturated TAGs (U3-TAG) (Table 2) (Zhang et al., 2014; Zhu et al., 2023). The LMMW-S3-TAG content was highest in the four AMFs at about 30%, followed by HMW-S2U1-TAG and LMMW-S2U1-TAG, each accounting for about 20%, while the U3-TAG level was the lowest at only 2%. In general, the TAGs rich in LC-FAs and SFAs displayed high MPs, while these values were lower in those rich in polyunsaturated FAs (Scrimgeour, Gao, Oh, & Shahidi, 2020). However, although B-AMF contained the most HMW-S3-TAGs, its SMP was not the highest, while A-AMF had fewer HMW-S3-TAGs but showed the highest SMP, which was ascribed to the highest level of S3-TAG with 48 to 54 carbon atoms (UHMM-S3-TAG) in the A-AMF. Moreover, it could be observed that the S25 yield was directly proportional to the content of UHMW-S3-TAG, but not significantly correlated with HMW-S3-TAG level. Yao et al. (2020) reported that TAGs with higher MPs, such as SSS, formed seed crystals with higher MPs during early crystallization of cocoa butter and guided the subsequent crystallization. Pratama, Simone, and Rappolt (2021) showed that long-chain saturated TAGs with higher MPs, such as SPS and PPS, provided higher thermodynamic driving force for nucleation during the cooling profiles. That was, UHMW-S3-TAG with higher SMPs played the role of seed crystals at the early crystallization stage of AMF to promote the co-crystallization of other TAGs, increasing the yield of S25.

The four L25s all displayed lower HMW-S3-TAG and HMW-S2U1-TAG levels, while the content of the other TAG groups was higher. The S25s exhibited the opposite trend (Table 2). Actually, the HMW-S3-TAGs and S2U1-TAGs with 48 to 54 carbon atoms (UHMW-S2U1-TAG) were mainly lower in the L25s and higher in the S25s (Fig. 3), illustrating that these two TAGs were primarily responsible for crystallization during fractionation. The UHMW-S2U1-TAGs displayed a higher SMP and crystallization capacity than LMMW-S3-TAGs. Contrary to the trend of AMFs, the content of UHMW-S3-TAG was lowest in A-L25 and highest in B-L25, indicating that a higher UHMW-S3-TAG level in the

Table 1
The FA composition of the AMFs from different sources and their fractions.

FAs	L25				AMF				S25			
	A	B	C	D	A	B	C	D	A	B	C	D
C4:0	1.67 ± 0.24[a]	1.82 ± 0.43[a]	2.07 ± 0.15[a]	1.97 ± 0.45[a]	1.39 ± 0.07[b]	1.63 ± 0.27[ab]	1.94 ± 0.07[a]	1.86 ± 0.30[a]	1.07 ± 0.38[b]	1.28 ± 0.09[ab]	1.67 ± 0.18[a]	1.70 ± 0.14[a]
C6:0	1.95 ± 0.26[a]	2.10 ± 0.42[a]	2.34 ± 0.15[a]	2.20 ± 0.43[a]	1.65 ± 0.07[b]	1.92 ± 0.27[ab]	2.21 ± 0.05[a]	2.12 ± 0.29[a]	1.3 ± 0.39[b]	1.56 ± 0.09[ab]	1.97 ± 0.22[a]	2.00 ± 0.08[a]
C8:0	1.68 ± 0.25[a]	1.79 ± 0.32[a]	2.00 ± 0.10[a]	1.85 ± 0.30[a]	1.44 ± 0.06[b]	1.66 ± 0.21[ab]	1.91 ± 0.04[a]	1.80 ± 0.20[a]	1.17 ± 0.28[b]	1.41 ± 0.06[ab]	1.73 ± 0.19[a]	1.73 ± 0.06[a]
C10:0	3.54 ± 0.43[a]	3.61 ± 0.45[a]	3.84 ± 0.17[a]	3.63 ± 0.45[a]	3.22 ± 0.16[b]	3.47 ± 0.32[ab]	3.82 ± 0.05[a]	3.65 ± 0.33[ab]	2.85 ± 0.30[b]	3.19 ± 0.12[ab]	3.78 ± 0.48[a]	3.68 ± 0.15[a]
C11:0	0.19 ± 0.04[a]	0.12 ± 0.01[b]	0.15 ± 0.01[b]	0.12 ± 0.02[b]	0.18 ± 0.01[a]	0.11 ± 0.01[c]	0.15 ± 0.01[b]	0.12 ± 0.01[c]	0.16 ± 0.02[a]	0.11 ± 0.01[b]	0.14 ± 0.01[a]	0.11 ± 0.01[b]
C12:0	3.97 ± 0.43[b]	5.00 ± 0.47[a]	4.22 ± 0.22[ab]	3.97 ± 0.49[b]	3.79 ± 0.24[b]	4.95 ± 0.34[a]	4.31 ± 0.08[b]	4.13 ± 0.36[b]	3.60 ± 0.09[b]	4.85 ± 0.10[a]	4.50 ± 0.59[a]	4.36 ± 0.17[a]
C13:0	0.30 ± 0.05[a]	0.18 ± 0.02[b]	0.24 ± 0.02[ab]	0.20 ± 0.03[b]	0.29 ± 0.03[a]	0.18 ± 0.02[c]	0.25 ± 0.01[b]	0.20 ± 0.02[c]	0.29 ± 0.01[a]	0.18 ± 0.01[c]	0.25 ± 0.03[b]	0.21 ± 0.01[c]
C14:0	9.12 ± 0.90[a]	9.68 ± 0.62[a]	9.67 ± 0.49[a]	9.47 ± 1.09[a]	9.12 ± 0.69[a]	9.92 ± 0.47[a]	10.11 ± 0.17[a]	10.00 ± 0.76[a]	9.12 ± 0.45[b]	10.37 ± 0.18[a]	10.97 ± 1.18[a]	10.8 ± 0.26[a]
C15:0	2.07 ± 0.21[a]	2.07 ± 0.08[a]	1.97 ± 0.12[a]	2.16 ± 0.15[a]	2.13 ± 0.13[ab]	2.18 ± 0.07[ab]	2.08 ± 0.05[b]	2.29 ± 0.09[a]	2.21 ± 0.05[b]	2.39 ± 0.06[a]	2.28 ± 0.09[b]	2.49 ± 0.02[a]
C16:0	21.87 ± 0.93[ab]	21.46 ± 0.42[b]	21.06 ± 0.57[b]	23.00 ± 0.93[a]	22.74 ± 1.05[b]	22.56 ± 0.36[b]	22.16 ± 0.10[b]	24.28 ± 0.69[a]	23.73 ± 1.19[b]	24.68 ± 0.25[b]	24.3 ± 0.90[b]	26.23 ± 0.38[a]
C17:0	0.92 ± 0.05[c]	1.62 ± 0.12[a]	1.14 ± 0.08[b]	1.65 ± 0.10[a]	1.04 ± 0.04[c]	1.66 ± 0.08[a]	1.15 ± 0.05[b]	1.68 ± 0.05[a]	1.17 ± 0.04[b]	1.72 ± 0.01[a]	1.17 ± 0.12[b]	1.74 ± 0.03[a]
C18:0	12.06 ± 1.10[a]	11.02 ± 0.74[a]	11.81 ± 0.46[a]	12.11 ± 1.07[a]	13.41 ± 0.64[a]	11.85 ± 0.60[b]	12.51 ± 0.14[ab]	12.76 ± 0.72[ab]	14.96 ± 0.23[a]	13.44 ± 0.40[b]	13.88 ± 1.15[ab]	13.75 ± 0.19[ab]
C14:1	1.75 ± 0.24[b]	2.24 ± 0.16[a]	1.89 ± 0.13[ab]	1.87 ± 0.23[ab]	1.57 ± 0.13[b]	2.08 ± 0.12[a]	1.79 ± 0.05[b]	1.77 ± 0.15[b]	1.36 ± 0.01[c]	1.78 ± 0.04[a]	1.59 ± 0.15[b]	1.62 ± 0.04[b]
C16:1	3.35 ± 0.15[b]	3.67 ± 0.14[a]	3.12 ± 0.10[b]	3.29 ± 0.08[b]	3.10 ± 0.10[b]	3.45 ± 0.11[a]	2.92 ± 0.05[c]	3.05 ± 0.04[b]	2.82 ± 0.04[b]	3.03 ± 0.07[a]	2.55 ± 0.05[d]	2.69 ± 0.02[c]
C17:1	0.49 ± 0.01[d]	0.70 ± 0.03[b]	0.53 ± 0.01[c]	0.85 ± 0.01[a]	0.45 ± 0.01[d]	0.65 ± 0.02[b]	0.49 ± 0.01[c]	0.77 ± 0.01[a]	0.41 ± 0.02[c]	0.54 ± 0.01[b]	0.40 ± 0.05[c]	0.65 ± 0.00[a]
C18:1	28.58 ± 2.46[a]	26.31 ± 1.63[a]	26.94 ± 1.21[a]	25.55 ± 2.55[a]	28.25 ± 1.41[a]	25.46 ± 1.2[b]	25.72 ± 0.28[b]	24.01 ± 1.78[b]	27.87 ± 0.39[a]	23.81 ± 0.43[b]	23.31 ± 1.89[bc]	21.66 ± 0.60[c]
C18:2	6.00 ± 0.46[a]	5.50 ± 0.55[ab]	6.14 ± 0.38[a]	4.76 ± 0.55[b]	5.76 ± 0.32[a]	5.25 ± 0.38[a]	5.73 ± 0.11[a]	4.33 ± 0.36[b]	5.49 ± 0.22[a]	4.77 ± 0.10[b]	4.91 ± 0.66[ab]	3.69 ± 0.08[c]
C18:3	0.50 ± 0.06[c]	1.12 ± 0.10[a]	0.87 ± 0.07[b]	1.34 ± 0.18[a]	0.47 ± 0.04[c]	1.03 ± 0.07[a]	0.78 ± 0.05[b]	1.17 ± 0.12[a]	0.43 ± 0.03[c]	0.87 ± 0.03[a]	0.61 ± 0.09[b]	0.91 ± 0.05[a]
SC-SFA	3.63 ± 0.50[a]	3.92 ± 0.86[a]	4.41 ± 0.30[a]	4.17 ± 0.88[a]	3.04 ± 0.13[b]	3.55 ± 0.55[ab]	4.15 ± 0.12[a]	3.98 ± 0.58[a]	2.46 ± 0.66[b]	2.97 ± 0.15[ab]	3.70 ± 0.41[a]	3.72 ± 0.14[a]
MC-SFA	9.38 ± 1.15[a]	10.51 ± 1.24[a]	10.21 ± 0.48[a]	9.58 ± 1.23[a]	8.63 ± 0.45[b]	10.19 ± 0.87[a]	10.19 ± 0.15[a]	9.70 ± 0.88[ab]	7.78 ± 0.64[b]	9.56 ± 0.26[a]	10.15 ± 1.27[a]	9.88 ± 0.39[a]
LC-SFA	46.34 ± 0.95[b]	46.03 ± 0.37[b]	45.89 ± 0.65[b]	48.6 ± 1.12[a]	48.73 ± 1.23[b]	48.34 ± 0.25[b]	48.24 ± 0.16[b]	51.22 ± 0.85[a]	51.47 ± 1.55[b]	52.79 ± 0.11[b]	52.85 ± 0.90[b]	55.21 ± 0.43[a]
USFA	40.66 ± 2.59[a]	39.55 ± 2.14[a]	39.49 ± 1.41[a]	37.65 ± 2.96[a]	39.6 ± 1.55[a]	37.93 ± 1.51[ab]	37.42 ± 0.35[ab]	35.1 ± 2.06[b]	38.38 ± 0.62[a]	34.80 ± 0.46[b]	33.36 ± 2.53[bc]	31.22 ± 0.70[c]

[a] The values were expressed as the mass percentage of individual FAs, g/100 g (means ± SD, $n = 3$).
[b] L25: liquid fraction fractionated at 25 °C; AMF: anhydrous milk fat; S25: solid fraction fractionated at 25 °C; SC-SFA: short-chain saturated fatty acids (C4:0 ~ C6:0); MC-SFA: medium-chain saturated fatty acids (C8:0 ~ C12:0); LC-SFA: long-chain saturated fatty acids (>C13:0); USFA: unsaturated fatty acids.
[c] Different letters in the same row of the same fractions represent significant differences ($P < 0.05$).

AMF would crystallize in the process the constant temperature, and be more seperated into S25 during fractionation. However, no significant differences were observed between the UHMM-S3-TAG content of the four S25s, which was because the higher yield of S25 involved a higher degree of low-melting TAG co-crystallization. This decreased its otherwise higher UHMW-S3-TAG proportion, therefore reducing the differences between the S25s and also resulting in the lower SMPs of both fractions.

3.4. Crystal morphology

TAGs mainly display α, β′, and β crystal forms, and their stabilities and SMPs increased from α, β′, to β forms. β crystals are typically needle-shaped, while β′ crystals are bulky, and α crystals present as tiny amorphous aggregates formed by melted fat due to rapid cooling (Himawan et al., 2006; Mao, Gao, & Meng, 2023). At 15 °C, the AMFs mainly appeared as fan-shaped bulky β' crystals with diameters of about 50–100 μm, and a few compact spherulites consisting of needle-like β crystals, with smaller diameters of about 20 μm, which were clearer in the micrographs of the diluted samples (Fig. 4). In the rapid cooling and sufficient holding time conditions adopted in this experiment, these crystals were more likely to be recrystallized from unstable α crystals (Cisneros, Mazzanti, Campos, & Marangoni, 2006; Himawan et al., 2006; Sato & Ueno, 2011). Pratama et al. (2021) revealed that TAGs containing uniform or symmetrical FAs, such as SSS, PPP, and SPS, mostly follow typical α → β' → β transformation. However, asymmetrical TAGs in which solitary SFAs or USFA reside in either the sn-1 or sn-3 position and TAGs with acyl chain length differences exceeding two carbon atoms, such as SSO, PPO, and PPM, are mostly stabilized as β' polymorphs. Due to the TAG composition diversity in the AMFs, they presented a β'/β crystal mixture dominated by the β' form. The A-AMF displayed more β spherulites, which was associated with higher PPP, PPS, and SPS abundance (Fig. 3). The L25 fractions exhibited sparse crystallization with large voids, while only bulky β' crystals were observed. The S25s produced denser needle-like β crystal networks with almost no voids, which were related to their content differences in the HMW-S3-TAGs and UHMM-S2U1-TAGs.

The L25s hardly formed crystals at 25 °C, except for B-L25, which

Table 2
The TAG composition of the AMFs from different sources and their fractions.

TAG	L25				AMF				S25			
	A	B	C	D	A	B	C	D	A	B	C	D
HMW-S3-TAG	5.53 ± 0.06[c]	6.84 ± 0.11[a]	5.56 ± 0.04[c]	6.14 ± 0.18[b]	10.70 ± 0.09[c]	11.66 ± 0.25[a]	9.55 ± 0.13[d]	11.26 ± 0.15[b]	16.63 ± 0.14[d]	20.96 ± 0.58[a]	17.36 ± 0.36[c]	19.04 ± 0.11[b]
LMMW-S3-TAG	30.10 ± 0.23[d]	33.16 ± 0.37[b]	31.75 ± 0.64[c]	36.98 ± 0.15[a]	27.89 ± 0.20[d]	30.78 ± 0.45[b]	29.95 ± 0.51[c]	34.41 ± 0.24[a]	25.34 ± 0.21[c]	26.19 ± 0.61[b]	26.41 ± 0.25[b]	30.51 ± 0.40[a]
HMW-S2U1-TAG	19.00 ± 0.23[a]	18.01 ± 0.29[b]	16.79 ± 0.42[c]	16.80 ± 0.09[c]	19.54 ± 0.11[a]	18.77 ± 0.22[b]	17.42 ± 0.30[c]	17.28 ± 0.13[c]	20.16 ± 0.07[a]	20.23 ± 0.11[a]	18.64 ± 0.08[b]	18.01 ± 0.30[c]
LMMW-S2U1-TAG	21.70 ± 0.28[c]	22.59 ± 0.07[b]	23.10 ± 0.12[a]	22.94 ± 0.17[a]	19.84 ± 0.13[d]	20.45 ± 0.13[c]	21.58 ± 0.10[a]	21.06 ± 0.16[b]	17.71 ± 0.04[b]	16.32 ± 0.31[c]	18.61 ± 0.24[a]	18.21 ± 0.23[a]
S1U2-TAG	18.65 ± 0.09[a]	15.50 ± 0.05[c]	17.66 ± 0.17[b]	13.68 ± 0.09[d]	17.52 ± 0.04[a]	14.77 ± 0.06[c]	16.77 ± 0.10[b]	12.85 ± 0.11[d]	16.23 ± 0.06[a]	13.37 ± 0.09[c]	15.02 ± 0.06[b]	11.59 ± 0.17[d]
U3-TAG	2.63 ± 0.04[a]	1.78 ± 0.02[b]	2.61 ± 0.07[a]	1.47 ± 0.04[c]	2.35 ± 0.02[a]	1.65 ± 0.02[b]	2.41 ± 0.05[a]	1.35 ± 0.03[c]	2.03 ± 0.02[a]	1.40 ± 0.03[b]	2.03 ± 0.03[a]	1.15 ± 0.01[c]
UHMW-S3-TAG	0.58 ± 0.02[c]	0.80 ± 0.02[a]	0.66 ± 0.03[b]	0.63 ± 0.02[b]	3.29 ± 0.06[a]	2.76 ± 0.09[bc]	2.68 ± 0.08[c]	2.90 ± 0.06[b]	6.40 ± 0.10[a]	6.55 ± 0.25[a]	6.65 ± 0.19[a]	6.35 ± 0.15[a]
UHMW-S2U1-TAG	9.76 ± 0.16[a]	7.75 ± 0.17[bc]	8.02 ± 0.25[b]	7.65 ± 0.01[c]	10.89 ± 0.06[a]	8.88 ± 0.14[b]	9.02 ± 0.19[b]	8.62 ± 0.06[c]	12.18 ± 0.25[a]	11.06 ± 0.08[b]	10.96 ± 0.06[b]	10.09 ± 0.15[c]

[a] The values were expressed as the mass percentage of individual TAGs (means ± SD, n = 3).
[b] L25: liquid fraction fractionated at 25 °C; AMF: anhydrous milk fat; S25: solid fraction fractionated at 25 °C; HMW-S3-TAG: trisaturated TAG with 41 to 54 carbon atoms; LMMW-S3-TAG: trisaturated TAG with 26 to 40 carbon atoms; HMW-S2U1-TAG: monounsaturated TAG with 41 to 54 carbon atoms; LMMW-S2U1-TAG: monounsaturated TAG with 28 to 40 carbon atoms; S1U2-TAG: diunsaturated TAG; U3-TAG: triunsaturated TAG; UHMW-S3-TAG: trisaturated TAG with 48 and 54 carbon atoms; UHMW-S2U1-TAG: monounsaturated TAG with 48 to 54 carbon atoms.
[c] Different letters in the same row of the same fraction represent significant differences ($P < 0.05$).

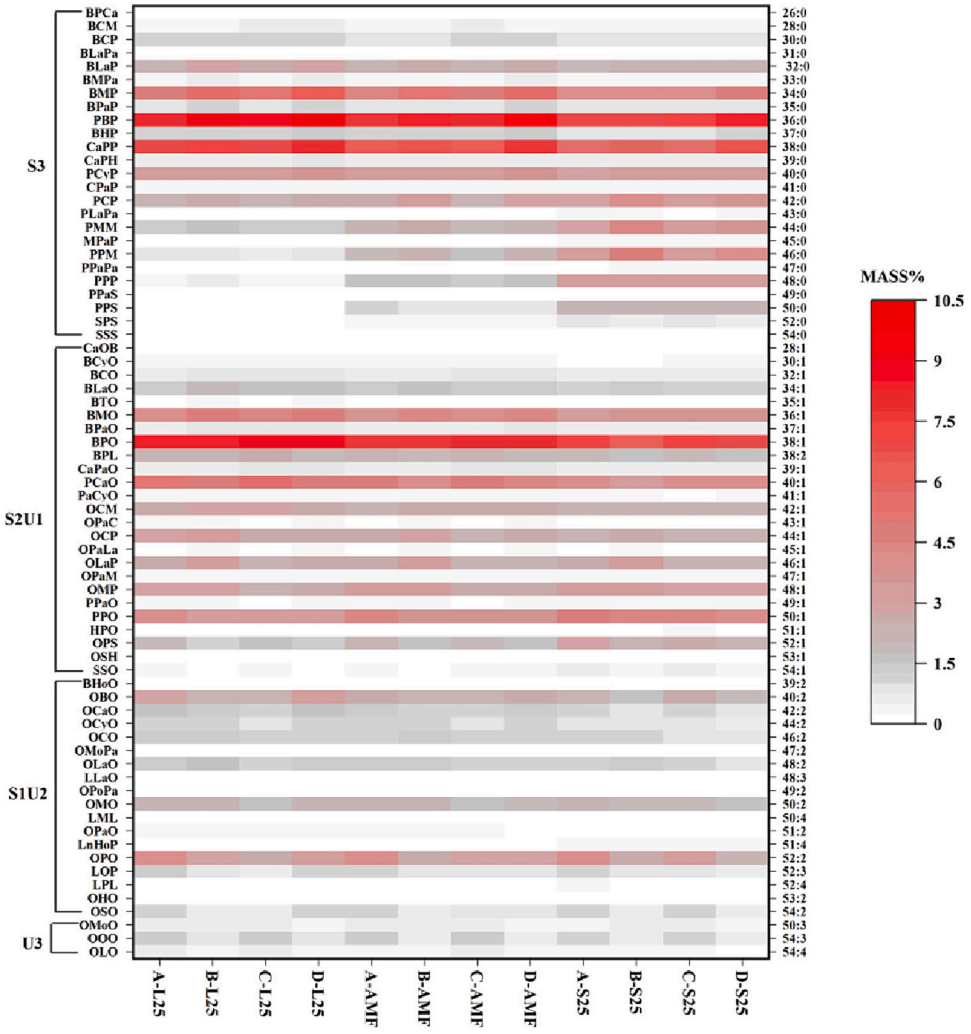

Fig. 3. A heat diagram of the TAGs in the AMFs from different sources and their fractions. Abbreviations: B: C4:0; Ca: C6:0; Cy: C8:0; C: C10:0; U: C11:0; La: C12:0; T: C13:0; M: C14:0; Mo: C14:1; Pa: C15:0; P: C16:0; Po: C16:1; H: C17:0; Ho: C17:1; S: C18:0; O: C18:1; L: C18:2; Ln: C18:3.

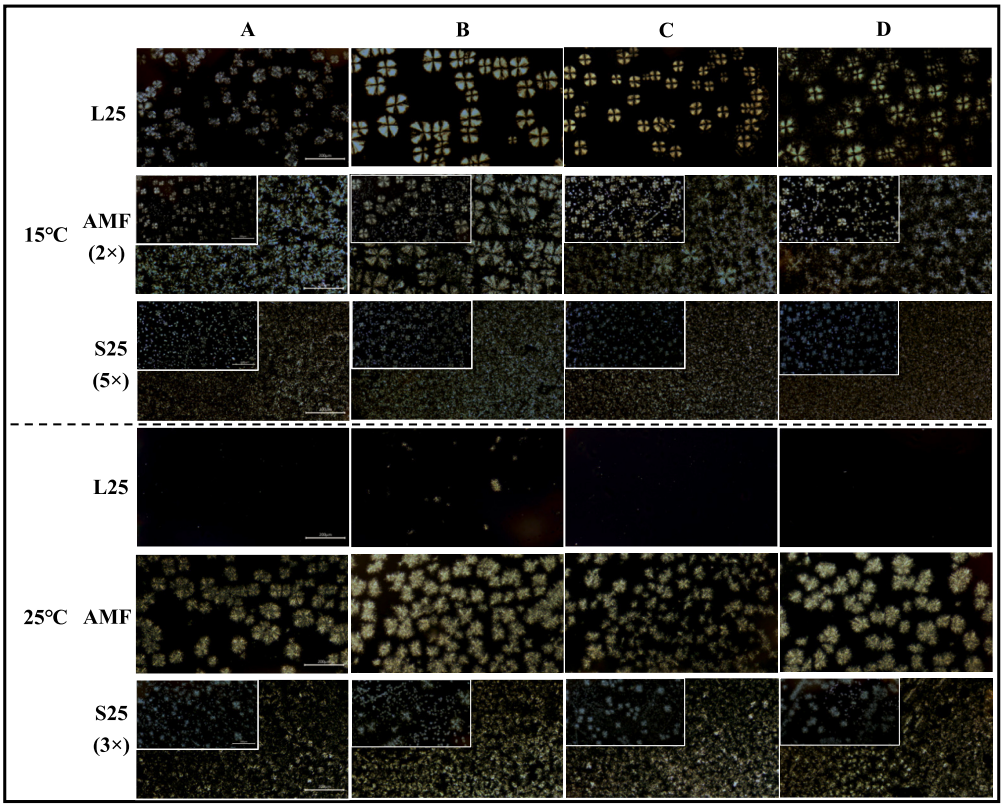

Fig. 4. The polarizing micrographs of the MFs from different sources, their fractions, and corresponding dilution system (upper left corner) at 15 °C and 25 °C. L25: liquid fraction fractionated at 25 °C; AMF: anhydrous milk fat; S25: solid fraction fractionated at 25 °C. The content in parentheses represents the dilution times (e.g., 2× indicates that a sample was diluted twice). The length of the line segment is 200 μm.

displayed a few β spherulites. However, they still contained a small number of HMM-S3-TAGs (5%), which are believed to require more significant supercooling for nucleation, while clustering is difficult in large samples (Zhang et al., 2014). Both the AMFs and S25s formed larger β spherulites, with diameters of about 50–100 μm and 20–100 μm, respectively. This might be because the high temperature provided energy for β' crystal transformation into β crystals, and the molten low-melting TAGs in the AMFs provided space for β-crystal migration and aggregation into spherulites (Zhang et al., 2014).

Although the TAG profile variation caused differences between the number of crystals in the four AMFs and fractions, this did not impact the overall similarity in the crystal morphology of the same fractions. The L25s only presented a few β' crystals at 15 °C, still maintaining a certain fluidity, while the S25s exhibited denser crystal networks and tended to form β crystals with higher stability at both 15 °C and 25 °C, which was consistent with their thermal properties.

4. Conclusion

Single-stage dry fractionation at 25 °C is used to separate four AMFs from different sources into L25s and S25s via pressure filtration, displaying satisfactory yields. The results show HMW-S3-TAG, UHMW-S2U1-TAG, and LC-SFA enrichment in the S25s, while the L25s exhibit SC-SFA, MC-SFA, and USFA abundance. Similar thermal and crystallization states are observed at 25 °C in the same fractions obtained from the four different AMFs. The L25s present a liquid with good fluidity and minimal crystals, while S25s are semi-solid, supported by β crystal networks with a certain hardness and plasticity.

However, the four AMFs produce different yields during dry fractionation, which is mainly influenced by UHMW-S3-TAGs. More UHMW-S3-TAGs in the AMF increase the S25 yield since they form seed crystals during early crystallization and promote the co-crystallization of the other TAGs. The increased co-crystallization of the TAGs in S25 decreased the co-crystallizable TAGs in L25, consequently lowering the SMPs of both fractions.

Although there are inevitably some differences between the AMFs from different sources and their fractions, their overall thermal and crystallization property similarities ensure that they provide the desired functional characteristics for the food industry. The L25s maintain good fluidity at room temperature and even at a lower temperature of 15 °C. Therefore, they can be used in cooking and spreadable products, such as sauces and butter, to provide a smoother taste and better ductility. The S25s remain thermally stable at room temperature, providing hardness and plasticity. Consequently, they are ideal alternatives for shortening, providing good formability and crispness to breads and cookies. They can also be combined with AMFs for whipping cream preparation to delay its collapse and mixed with cocoa butter to inhibit chocolate blooming.

CRediT authorship contribution statement

Yue Li: Writing – review & editing, Writing – original draft, Validation, Methodology, Formal analysis, Conceptualization. **Yan Li:** Writing – review & editing, Validation, Project administration, Methodology, Funding acquisition, Conceptualization. **Guosen Yan:** Software, Methodology, Investigation, Conceptualization. **Shiran Wang:** Methodology, Conceptualization. **Yunna Wang:** Conceptualization, Methodology. **Yang Li:** Conceptualization, Methodology. **Zhenbo Shao:** Resources. **Hui Wang:** Resources. **Liebing Zhang:** Conceptualization, Funding acquisition.

Declaration of competing interest

The authors declare that they have no known competing financial

interests or personal relationships that could have appeared to influence the work reported in this paper.

Data availability

Data will be made available on request.

Acknowledgments

This work was supported by the Agriculture Research System of China (No. CARS-36), the Key Research and Development Program of Ningxia Hui Autonomous Region (No. 2021BEF02031) and the National Natural Science Foundation of China (No. 32302137).

Appendix A. Supplementary data

Supplementary data to this article can be found online at https://doi.org/10.1016/j.fochx.2024.101350.

References

Chilliard, Y., Ferlay, A., & Doreau, M. (2001). Effect of different types of forages, animal fat or marine oils in cow's diet on milk fat secretion and composition, especially conjugated linoleic acid (CLA) and polyunsaturated fatty acids. *Livestock Production Science, 70*(1), 31–48.

Cisneros, A., Mazzanti, G., Campos, R., & Marangoni, A. G. (2006). Polymorphic transformation in mixtures of high- and low-melting fractions of milk fat. *Journal of Agricultural and Food Chemistry, 54*(16), 6030–6033.

Fatouh, A. E., Singh, R. K., Koehler, P. E., Mahran, G. A., El-Ghandour, M. A., & Metwally, A. E. (2003). Chemical and thermal characteristics of buffalo butter oil fractions obtained by multi-step dry fractionation. *LWT - Food Science and Technology, 36*(5), 483–496.

Fatouh, A. E., Singh, R. K., Koehler, P. E., Mahran, G. A., & Metwally, A. E. (2005). Physical, chemical and stability properties of buffalo butter oil fractions obtained by multi-step dry fractionation. *Food Chemistry, 89*(2), 243–252.

Gresti, J., Bugaut, M., Maniongui, C., & Bezard, J. (1993). Composition of molecular species of Triacylglycerols in bovine Milk fat. *Journal of Dairy Science, 76*(7), 1850–1869.

Guan, M., Dai, D., Li, L., Wei, J., Yang, H., Li, S., Zhang, Y., Lin, Y., Xiong, S., & Zhao, Z. (2017). Comprehensive qualification and quantification of triacylglycerols with specific fatty acid chain composition in horse adipose tissue, human plasma and liver tissue. *TALANTA, 172*, 206–214.

Himawan, C., Starov, V. M., & Stapley, A. G. F. (2006). Thermodynamic and kinetic aspects of fat crystallization. *Advances in Colloid and Interface Science, 122*(1–3), 3–33.

Larsen, M. K., Andersen, K. K., Kaufmann, N., & Wiking, L. (2014). Seasonal variation in the composition and melting behavior of milk fat. *Journal of Dairy Science, 97*(8), 4703–4712.

Lopez, C., Bourgaux, C., Lesieur, P., Riaublanc, A., & Ollivon, M. (2006). Milk fat and primary fractions obtained by dry fractionation: 1. Chemical composition and crystallisation properties. *Chemistry and Physics of Lipids, 144*(1), 17–33.

Lopez, C., & Ollivon, M. (2009). Triglycerides obtained by dry fractionation of milk fat: 2. Thermal properties and polymorphic evolutions on heating. *Chemistry and Physics of Lipids, 159*(1), 1–12.

Małkowska, M., Staniewski, B., & Ziajka, J. (2021). Analyses of milk fat crystallization and milk fat fractions. *International Journal of Food Properties, 24*(1), 325–336.

Mao, J., Gao, Y., & Meng, Z. (2023). Crystallization and phase behavior in mixture systems of anhydrous milk fat, palm stearin, and palm oil: Formation of eutectic crystals. *Food Chemistry, 399*, Article 133877.

Maurice-Van, E. M., Hiemstra, S. J., & Calus, M. P. (2011). Short communication: Milk fat composition of 4 cattle breeds in the Netherlands. *Journal of Dairy Science, 94*(2), 1021–1025.

Pacheco-Pappenheim, S., Yener, S., Goselink, R., Quintanilla-Carvajal, M. X., van Valenberg, H. J. F., & Hettinga, K. (2022). Bovine milk fatty acid and triacylglycerol composition and structure differ between early and late lactation influencing milk fat solid fat content. *International Dairy Journal, 131*, Article 105370.

Pratama, Y., Simone, E., & Rappolt, M. (2021). The unique crystallization behavior of Buffalo Milk fat. *Crystal Growth & Design, 21*(4), 2113–2127.

Precht, D., Molkentin, J., & de Froidmont-Gortz, I. (1998). Anhydrous butterfat reference material CRM519: Certification of triglyceride composition and cholesterol content including homogeneity and stability tests. *FETT-LIPID, 100*(12), 9.

Ren, Q., Li, L., Dudu, O. E., & Ma, Y. (2019). Thermal and structural changes of pasteurized milk fat globules during storage. *Food Bioscience, 28*, 27–35.

Sato, K., & Ueno, S. (2011). Crystallization, transformation and microstructures of polymorphic fats in colloidal dispersion states. *Current Opinion in Colloid & Interface Science, 16*(5), 384–390.

Scrimgeour, C., Gao, Y., Oh, W. Y., & Shahidi, F. (2020). Chemistry of fatty acids. In *Bailey's industrial oil and fat products* (pp. 1–40).

Sebben, D. A., Gao, N., Gillies, G., Beattie, D. A., & Krasowska, M. (2019). Fractionation and characterisation of hard milk fat crystals using atomic force microscopy. *Food Chemistry, 279*, 98–104.

Si, X., Zhu, H., Zhu, P., Wang, Y., Pang, X., Ju, N., … Zhang, S. (2023). Triacylglycerol composition and thermodynamic profiles of fractions from dry fractionation of anhydrous milk fat. *Journal of Food Composition and Analysis, 115*, Article 104916.

Wang, S., Li, Y., Yan, G., Yuan, D., Ji, B., Zhou, F., … Zhang, L. (2023). Thickening mechanism of recombined dairy cream stored at 4°C: Changes in the composition and structure of milk protein under different sterilization intensities. *International Journal of Biological Macromolecules, 227*, 903–914.

Wang, Y., Li, Y., Yuan, D., Li, Y., Payne, K., & Zhang, L. (2019). Effect of fractionation and chemical characteristics on the crystallization behavior of milk fat. *Journal of Food Science, 84*(12), 3512–3521.

Yan, G., Li, Y., Wang, H., He, L., Li, Y., Li, Y., Zhang, L., & Yan, J. (2023). Effect of composition of emulsifier blends on aerated emulsions: Stability, thermodynamic, interfacial behavior and aeration properties. *LWT, 188*, Article 115395.

Yao, Y., Liu, W., Zhang, D., Li, R., Zhou, H., Li, C., & Wang, S. (2020). Dynamic changes in the triacylglycerol composition and crystallization behavior of cocoa butter. *Food Science and Technology, 129*, Article 109490.

Yener, S., & van Valenberg, H. J. F. (2019). Characterisation of triacylglycerols from bovine milk fat fractions with MALDI-TOF-MS fragmentation. *TALANTA, 204*, 533–541.

Zhang, X., Li, L., Xie, H., Liang, Z., Su, J., Liu, G., & Li, B. (2014). Effect of temperature on the crystalline form and fat crystal network of two model palm oil-based shortenings during storage. *Food and Bioprocess Technology, 7*(3), 887–900.

Zhu, H., Si, X., Wang, Y., Zhu, P., Pang, X., Wang, X., … Lv, J. (2023). Fatty acid, triglyceride, and kinetic properties of milk fat fractions made by the combination of dry fractionation and short-path molecular distillation. *Journal of Dairy Science, 106*(10), 6655–6670.